Dynamics of Myosin-V Processivity

Ganhui Lan* and Sean X. Sun*†
*Department of Mechanical Engineering, and †Whitaker Institute of Biomedical Engineering, Johns Hopkins University, Baltimore, Maryland

ABSTRACT Myosin-V is an actin-associated processive molecular motor. Single molecule experiments revealed that myosin-V walks in a stepwise fashion with occasional backward steps. By combining the mechanical structure of the motor with the ATP hydrolysis kinetics, we construct a dynamical model that accounts for the stepwise processivity. The molecular properties of the protein chains connecting the myosin heads are important. A simple elastic model demonstrates that the stress transmitted from the leading head to the trailing head leads to net forward motion. The step-sizes are non-uniform. We also predict there are several substeps. The translational speed and step-size distributions are computed for several different conditions. The computed force-versus-velocity curve shows that under an external load, myosin-V slows down. However, the sizes of the steps remain the same.

INTRODUCTION

Unlike the single-headed myosins, myosin-V is a kinesin-like processive molecular motor (Howard, 2001; Mehta et al., 1999; Rief et al., 2000). In cells, myosin-V transports vesicles and organelles along actin filaments (Langford, 2002). ATP hydrolysis energy fuels the translational movement of myosin-V toward the plus end of actin. The processive motion has been observed in single-molecule experiments (Veigel et al., 2001; Tanaka et al., 2002; Yildiz et al., 2003; Purcell et al., 2002). Several mechanisms (Walker et al., 2000; Ishii and Yanagida, 2002) and theoretical models (Kolomeisky and Fisher, 2003) have been proposed to explain the observed data. In particular, the hand-over-hand mechanism seems to be consistent with the majority of the experimental evidence. In this article, we develop a three-dimensional quantitative model that explains the experimental observations. The model is motivated by the structure of the myosin-V complex. The mechanical energy transfer between the myosin heads is explicitly computed without assuming a hand-over-hand mechanism. We discover that the molecular property of the myosin-V subunits play an important role. We show that reasonable choices of parameters in our model leads to a hand-over-hand mechanism of myosin-V stepping. The forward movement is due to the enhancement of ADP release from the trailing head. Under an external load, binding to actin becomes rate-limiting, until stall is reached.

The principal structural difference between myosin-V and other single-head myosins is in regions away from the motor domain. Therefore, the hydrolysis mechanism and movement of the lever-arm for the ordinary myosin-II (Howard, 2001) is applicable to myosin-V. Bulk kinetic measurements of single myosin-V molecules show that this is indeed the case (de la Cruz et al., 1999). We conclude from available data that phosphate release leads to a powerstroke and a swinging of the lever arm (Raymond et al., 1993; Houdusse et al., 2000). In contrast with F_1-ATPase where ATP binding is the powerstroke step (Wang and Oster, 1998; Sun et al., 2004), myosins use ATP binding to release from actin. We note that the powerstroke motion is a change in the *average conformation* of motor domain. Due to thermal motion, there is always some fluctuation in the conformation of myosin-V. We postulate that after Pi release, there is a thermodynamic driving force (powerstroke) that rotates the light-chain domain with respect to the motor domain (see Fig. 1). At the moment, we cannot speculate the exact sequence of events that translate the movements in the binding pocket through the converter region to the lever arm. However, careful molecular dynamics simulations starting from high resolution structures can, perhaps, answer this question. In this article, we postulate the kinematics and energetics of the motor from known structural and kinetic data. Our goal is to quantitatively explain the mechanism that leads to the unidirectional motion of myosin-V.

CONSTRUCTION OF THE MODEL

Molecular motors can be viewed as stochastic systems undergoing random Brownian motion on a free energy surface (Mogilner et al., 2002; Bustamante et al., 2001). Myosin-V has two motor domains coupled by protein filaments (light-chains; see Fig. 1). Therefore a minimal description should include one mechanical variable and one chemical state variable for each motor domain. In our model, we focus on the following four variables: (θ_1, θ_2, s_1, and s_2), where $s_{1,\ 2}$ are the chemical states of the myosin heads 1 and 2, respectively, representing the various occupancies of the nucleotide and actin binding sites. Each motor domain can be in any 1 of 10 possible states and the total number of states for the motor complex is 10^2. (Fig. 2 shows the chemical states of a single head and the

Submitted June 14, 2004, and accepted for publication November 15, 2004.
Address reprint requests to Sean Sun, Tel.: 410-516-4003; E-mail: ssun@jhu.edu.

0006-3495/05/02/999/10 $2.00
doi: 10.1529/biophysj.104.047662

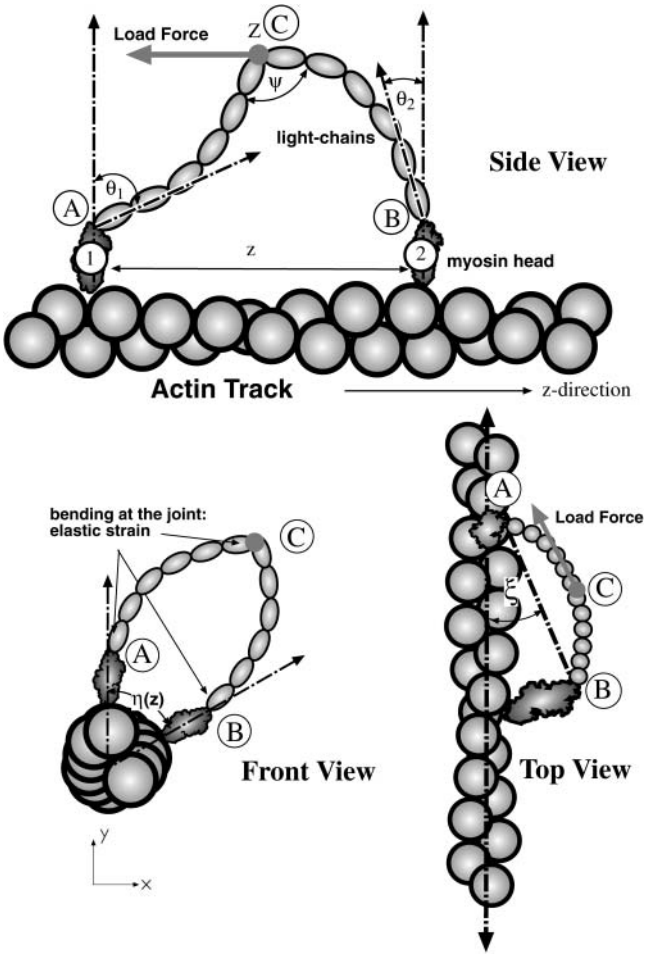

FIGURE 1 Three-dimensional arrangement of actin-myosin-V complex. The actin binding sites are shown as red spheres. The three mechanical joints in myosin-V are labeled as *A*, *B*, and *C*. The load force is applied at joint *C*. In our model, the load force is parallel to the *AB*-vector and has no vertical component.

allowed transitions to the neighboring states. No particular kinetic pathway is assumed. However, the mostly likely pathway given by the model is shown in *red*.) To define θ_i, we construct a vertical vector pointing along the myosin head and project it into the plane defined by points *A*, *B*, and *C*. The value θ_i is the geometric angle formed by the projected vector and the tangent vector of the light-chain filament at the joints *A* and *B* (see Fig. 1). The dynamics of these variables are given by a system of Langevin equations (Risken, 1989),

$$\zeta\dot{\theta}_i = -\frac{\partial E(\theta_1, \theta_2, s_1, s_2, F)}{\partial\theta_i} + f_B(t)$$

$$\frac{\partial\rho(s_1, s_2)}{\partial t} = \mathbf{K}(\theta_1, \theta_2, s_1, s_2)\times\rho(s_1, s_2), \qquad (1)$$

where ζ is the viscous friction experienced by the rotating light-chains and $f_B(t)$ is the random Brownian force, F is an external load force, and $\partial E(\theta_1, \theta_2, s_1, s_2, F)/\partial\theta_i$ is the total torque exerted on the light-chain. The torque is a function of the chemical state of the myosin heads as well as the overall mechanical state of the motor. The value $\rho(s_1, s_2)$ is a vector containing populations of the various chemical states. **K** is a matrix of transition rates connecting the chemical states. The transition rates are also functions of the mechanical variables (θ_i), indicating that the elastic energy in the overall motor complex can change the equilibrium constants and the reaction rates.

Myosin-V elastic energy

For a free myosin head with a fixed occupancy of catalytic and actin binding sites, the conformation of the motor and the angular positions of the light-chains can fluctuate according to an elastic energy $E_0(\theta_i, s_i)$. For two myosin heads, the protein chains linking the two heads can bend and distort. The total energy must include the elasticity of the light-chains. In addition, for each actin segment, there are two possible binding sites. Due to the helical nature of the actin strands, the binding sites rotate about the actin axis with a periodic repeat of 13×5.5 nm/2 = 36 nm. A myosin taking a step that is different from 36 nm must step around actin. This creates elastic strain in the joint between the motor domain and the light-chains.

To model the elastic energy of the motor complex, we assume that the angle, ψ, between the light-chains at *C* is free to rotate within the plane define by points *A*, *B*, and *C*. EM (electron microscopy) photos of myosin-V indicate that this is a reasonable assumption (Burgess et al., 2002). Fig. 1 shows the geometry of problem from several different view points. (Because the persistence length of actin is 15 μm, we assume actin is rigid.) We write the total elastic energy of myosin-V as a sum of four terms,

$$E(\theta_1, \theta_2, s_1, s_2) = E_0(\theta_1, s_1) + E_0(\theta_2, s_2) + E_l(\theta_1, \theta_2, z, F) + E_z(z), \qquad (2)$$

where z is the relative separation between the myosin heads (see Fig. 1). We now examine each term separately.

E_0

$E_0(\theta_i, s_i)$ is the elastic energy of a single myosin head. Here, we have assumed that the conformation is characterized by θ and can fluctuate according to E_0. This energy depends on the chemical state of the myosin head, s_i. Thus, binding, hydrolysis, and release of nucleotides give rise to changes in the conformation. We assume that the rough shape of E_0 is only a function of the catalytic site occupancy and does not depend on whether actin is bound. Thus, we have five different functions representing empty (*.E), loosely bound ATP (*.T*), tightly bound ATP (*.T), ADP.Pi (*.DP), and ADP (*.D) occupancies. These potentials are displayed in

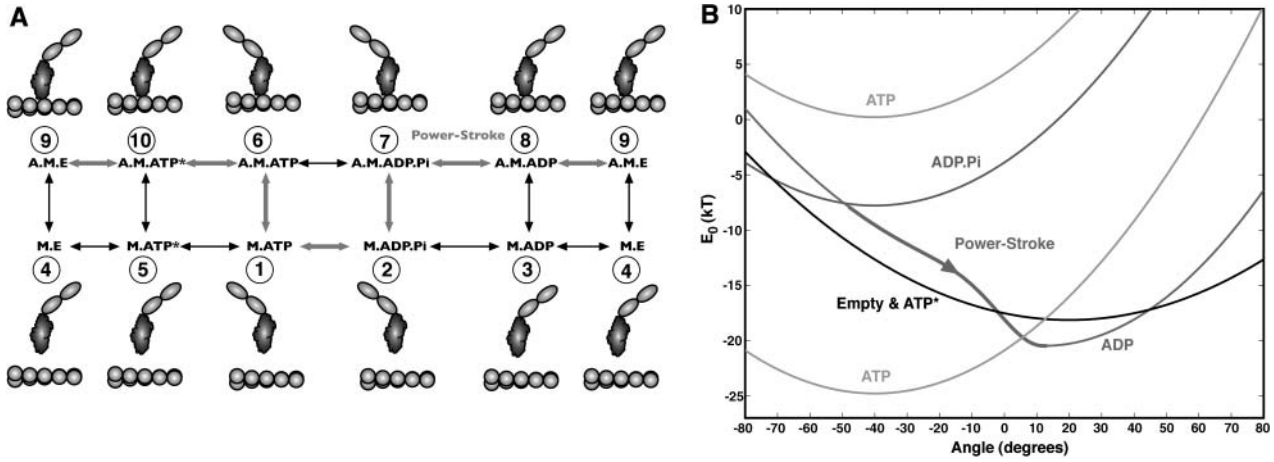

FIGURE 2 The kinetic cycle in a single myosin-V motor domain: (*A*) Ten possible occupancy states of a single myosin are shown, along with the approximate equilibrium geometry of the lever-arm. The transition rates between these states are given in the section ''Myosin-V kinetics''. The preferred pathway revealed by our model is given by the red path, although other pathways are also possible. The cartoons illustrate the preferred conformations of the motor domain. (*B*) The elastic energy versus the angular position of the light-chain, $E_0(\theta_i, s_i)$, for a single actin-free myosin head. The energies are the same for actin-bound heads, except for an additive constant. Chemical transitions between states are specified in the section ''Myosin-V kinetics''. The equilibrium conformation for each chemical state corresponds to the lowest energy configurations (see *A*).

Fig. 2. In the D-, E-, and T*-states, the preferred angles of the lever arm are positive, indicating that the light-chains are pointing forward. In the T- and DP-states, the preferred angle of the lever arm are negative. The powerstroke occurs after Pi release on the D-state (see Fig. 2).

For most of the chemical states, we model E_0 with a harmonic potential

$$E_0(\theta_i, s_i) = \frac{1}{2}k(s_i)[\theta_i - \theta_0(s_i)]^2 + c(s_i), \qquad (3)$$

where $k(s_i)$ and $\theta_0(s_i)$ are the force constant and preferred angle of the harmonic oscillator, respectively. The value $c(s_i)$ is a constant accounting for the free energy difference between the states. The value $c(s_i)$ can be obtained from measured kinetic rate constants using the detailed balance condition

$$\frac{k^0_{s_i \to s_i'}}{k^0_{s_i' \to s_i}} = \exp\left[\frac{E_0(\theta_0(s_i), s_i) - E_0(\theta_0(s_i'), s_i')}{k_B T}\right], \qquad (4)$$

where $k^0_{s_i \to s_i}$ are the experimentally measured rate constants. These rate constants are summarized in Table 3. For $s_i =$ (*.D), the potentials are given by an alternative function,

$$E_0(\theta_i, *.\mathrm{D}) = \begin{cases} A[e^{-b(\theta_i - \theta_0(*.\mathrm{D}))^2} - 1] + B[\theta_i - \theta_0(*.\mathrm{D})]^2 + c(*.\mathrm{D}) & \text{if} \quad \theta_i \le \theta_0(*.\mathrm{D}) \\ \frac{1}{2}k(*.D)[\theta_i - \theta_0(*.\mathrm{D})]^2 + c(*.\mathrm{D}) & \text{if} \quad \theta_i > \theta_0(*.\mathrm{D}) \end{cases}, \qquad (5)$$

where $A = -6\ k_BT$, $b = 10.0$, and $B = 6\ k_BT$. The value $E_0(\theta_i$, A.M.D) differs from $E_0(\theta_i$, M.D) by a constant. Our choice for $E_0(\theta_i$, *.D) is a hypothesis, due to our observation that the simple harmonic form of Eq. 3 does not produce enough torque near equilibrium. The actual functional form can only be determined from careful experiments. Given our choice, at the end of the power-stroke, the system locks into a preferred configuration. Thus, the powerstroke motion when the motor is in the *.D-state is akin to a ratchet. Table 1 lists all the parameters used to specify the states.

E_l

$E_l(\theta_1, \theta_2, z, F)$ represents the light-chain elastic energy in the ABC plane. This energy is a function of the in-plane curvature of the light-chain filaments. For given angles (θ_1, θ_2) and the relative separation between the heads, z, the light-chains are assumed to be in mechanical equilibrium. The equilibrium configuration of the light-chains, which gives the position of the joint C, are computed from a semiflexible filament model (Doi and Edwards, 1986).

To compute E_l, we first consider the situation where both myosin motors are bound to actin. The light-chains are α-helices with six bound calmodulins. If the vectors $\mathbf{r}_i$ and $\mathbf{r}'_i$ define the orientations of the i^{th} calmodulin subunit in chains 1 and 2, respectively, then the elastic energy of two inextensible and semiflexible filaments are given by

TABLE 1 Parameters used in the definitions of $E_0(\theta_i, s_i)$

s_i	Identity	$k(s_i)(k_BT/\text{rad}^2)$	$\theta_0(s_i)$ (degrees)	$c(s_i)(k_BT)$
1	M.E	10.0	20	−5.0812
2	M.ATP*	10.0	20	−5.8389
3	M.ATP	16.0	−40	0.0 (−25.0)
4	M.ADP.Pi	16.0	−40	−2.0
5	M.ADP	20.0	12	−8.6931
6	A.M.E	10.0	20	−18.1054
7	A.M.ATP*	10.0	20	−18.1393
8	A.M.ATP	16.0	−40	0.2126
9	A.M.ADP.Pi	16.0	−40	−7.7874
10	A.M.ADP	20.0	12	−20.4805

The differences in the $c(s_i)$ are the measured free energy differences between chemical states.

$$E_l = -k_BT\sum_{i=2}^{6}\frac{l_p}{a^3}[\mathbf{r}_i\cdot\mathbf{r}_{i-1}+\mathbf{r}'_i\cdot\mathbf{r}'_{i-1}-2a^2]+C(\mathbf{r}_6,\mathbf{r}'_6), \tag{6}$$

where l_p is the persistence length of the filament. $C(\mathbf{r}_6,\mathbf{r}'_6)$ is the constraint $\mathbf{r}_6=\mathbf{r}'_6$. The dependence on θ_1, θ_2, and z is contained in $\mathbf{r}_1$ and $\mathbf{r}'_1$. The vectors $\mathbf{r}_1$ and $\mathbf{r}'_1$ are fixed by their angular positions and the relative separations. The values of the parameters a and l_p, along with other constants, are given in Table 2. Because the filaments are inextensible, $|\mathbf{r}_i|\equiv a$ is a constant. The relative orientations of the segments are given by

$$\mathbf{r}_i=\mathbf{R}(\chi_i)\cdot\mathbf{r}_{i-1}, \tag{7}$$

where $\mathbf{R}(\chi_i)$ is a one-parameter rotation matrix. For any given θ_1, θ_2, and z, it is possible to minimize E_l with respect to the χ_i values and obtain an equilibrium chain configuration and an equilibrium energy. The equilibrium energy as a function of θ_1, θ_2, and z is defined as E_l.

With an external force, $\mathbf{F}$, the total elastic energy becomes

$$E_l = -k_BT\sum_{i=2}^{6}\frac{l_p}{a^3}[\mathbf{r}_i\cdot\mathbf{r}_{i-1}+\mathbf{r}'_i\cdot\mathbf{r}'_{i-1}-2a^2] - \mathbf{F}\cdot\mathbf{r}_6+C(\mathbf{r}_6,\mathbf{r}'_6). \tag{8}$$

TABLE 2 Miscellaneous parameters used in the model

Parameter	Description	Value
$D_{1,2}$	Diffusion constants of $\theta_{1,2}$	5.5×10^4 rad^2/s
η	Viscosity of water	1×10^{-9} pN/s per nm^2
M	Force constant for E_z	120 k_BT
l_m	Length of the myosin head	6.6 nm
r_a	Radius of the actin filament	5.5 nm
r_0	Radius of the light-chains	2.5 nm
l_p	The persistence length of the light-chains	120 nm
a	Length of the light-chain segments (calmodulin)	5.0 nm
L	Total length of the light-chains, $6a$	30 nm

We model the situation where the external force is coming from a spherical laser-trap. Thus, $\mathbf{F}$ always lies in the plane defined by A, B, and C. We also assume that the force has no vertical component perpendicular to the actin axis. (In a typical laser-trap operating on a bead, the applied force will have some vertical component. We have not considered this situation.) With this geometry, the work done by the force is then $-FZ$ where Z is the position of point C along the AB-vector. Notice that the configurations of the light-chains are functions of the external force; therefore, E_l has to be computed for each load force.

If only one myosin motor is bound to actin, then the elastic energy is given by

$$E'_l = -k_BT\sum_{i=2}^{6}\frac{l_p}{a^3}(\mathbf{r}_i\cdot\mathbf{r}_{i-1}-a^2)-\mathbf{F}\cdot\mathbf{r}_6, \tag{9}$$

where the sum is only over one filament. Since we assume that the joint at point C is free, light-chain 2 is free to diffuse. We do not explicitly compute the position of the second light-chain in this situation. Notice that the new equilibrium position Z' will be significantly different from Z when both heads are bound to actin. In fact, $Z-Z'\approx11$ nm; it is one of the observed substeps.

E_z

$E_z(z)$ is the elastic energy as a function of the relative z distance between the bound heads. From Fig. 1, we see that depending on the binding site of the leading head, the light-chain filaments can curve away from the actin axis. This additional curvature energy, and the elastic strain at joints A, B, and C are defined as E_z. Taking advantage of the fact that ξ is small, we assume a simple small deformation model. If $z=36$ nm, then $\xi=0$. As the leading head binds away from $z=36$ nm, ξ increases. We write

$$E_z(z)=\frac{1}{2}M\xi^2(z), \tag{10}$$

where the geometrical relationship between ξ and z is

$$\xi(z)=\tan^{-1}\left[\frac{2(l_m+r_a)\sin\eta(z)/2}{z}\right]. \tag{11}$$

If the light-chains are isotropic rods, then M is related to l_p defined for E_1. However, we find that the light-chains must be anisotropic, and bending elastic energy away from actin is quite high. The force constant M, the length of the myosin head l_m, and the radius of the actin filament r_a are given in Table 2. The value η is defined in Fig. 1 *B*. Notice that the z distance along the actin axis is not the same as the distance along the AB-vector. This geometry is taken into account explicitly. Fig. 3 shows $E_z(z)$ used in the model.

The elastic energy in the myosin-V complex is how the movements of the two heads are regulated. When the leading head makes a powerstroke, a torque is experienced by the trailing head. This torque changes the ADP release rate in

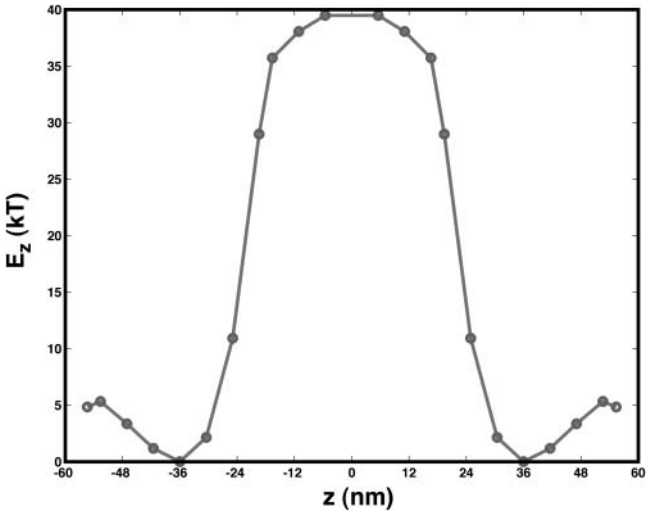

FIGURE 3 E_z as a function of z. E_z is defined in Eq. 10.

the trailing head to accelerate unbinding from actin. The elastic energy also regulates binding to actin. The rate of binding to actin is a function of z, indicating that myosin-V takes regular steps.

Myosin-V kinetics

The catalytic activity of single-headed myosin-V has been studied (de la Cruz et al. 1999). Many of the intermediate reaction rates have been measured. The measured rate constants are summarized in Table 3. We include all the observed kinetic states and use the experimental rate constants to parameterize our model. The reaction rates between the states depend on θ_i. The measured reaction rates are for a single-headed myosin-V where θ_i is at equilibrium.

The kinetic rate constants for myosin-V can be classified into two groups: *Group one* involves changes in chemical state of the catalytic site; *Group two* involves binding and unbinding to actin. For reactions without changes in the actin affinity, we have assumed that the rate constants depend on the angular position as

$$k_{s_i \to s_i'}(\theta_i) = k^0_{s_i \to s_i} e^{-(E_0(\theta_i, s_i) - E_0(\theta_0(s_i), s_i))/k_B T} \quad (12)$$

for the forward reactions. In essence, we postulate that the catalytic activity of the enzyme is the greatest when the conformation is the most energetically favorable. For the reverse reaction, the detailed-balance condition is utilized as

$$\frac{k_{s_i \to s_i'}}{k_{s_i' \to s_i}} = \exp[\beta(E_0(\theta_i, s_i) - E_0(\theta_i, s_i'))]. \quad (13)$$

Given the forward reaction expression of Eq. 12, Eq. 13 is used to solve for the reverse reaction rate.

For the transition from *.D → *.E, the reaction rate must depend on the configuration of the binding pocket. The rate of ADP release is enhanced if an external force can apply stress to the binding pocket. An interpolation movie of myosin II indicates that the movements of the pocket are correlated with the angular position of the lever arm. (The movie is generated from two conformations of scallop myosin II. An interpolation between the structures is carried out using Gerstein's Database of Macromolecular Movements; see http://www.molmovdb.org/MolMoveDB/. The movie is available for download at http://pegasus.me.jhu.edu/ seansun/myosinV.htm.) If the lever-arm swings forward, it appears that the pocket becomes more open. Thus, if an external torque is applied to the lever-arm and changes the angular position to $>\theta_0$(*.D), the ADP release rate should increase. To incorporate this effect, we write $k_{D \to E}$ as

$$k_{*.D \to *.E}(\theta_i) = \frac{\tanh[\sigma(\theta_i - \theta_0(*.D) - \Delta)] + 1}{\tanh[-\sigma\Delta] + 1}, \quad (14)$$

where $\sigma = 10.0$ and $\Delta = -3.5°$. The constants are chosen so that

$$k_{*.D \to *.E}(\theta_0(*.D)) = k^0_{*.D \to *.E}. \quad (15)$$

If $\theta_i > \theta_0(*.D)$, the ADP release rate is larger by approximately a factor of 2. This way of writing the reaction rate is essentially equivalent to the standard rate enhancement formula,

$$k_{*.D \to *.E}(\theta_i) = k^0_{*.D \to *.E} e^{\beta \tau_1 \Delta \theta_p}, \quad (16)$$

TABLE 3 Reaction rate matrix (s^{-1}) for a single myosin-V head, adapted from de la Cruz et al. (1999) and Howard (2001)

	M.T	M.DP	M.D	M.E	M.T*	A.M.T	A.M.DP	A.M.D	A.M.E	A.M.T*
M.T	–	89.4			750.0	2000				
M.DP	660.6	–	1.2×10^{-4}				14.4			
M.D		0.1	–	46.0				3.2×10^{-2}		
M.E			1.2	–	87.9				0.16	
M.T*	3.6×10^{-6}			187.5	–					0.33
A.M.T	1616.9					–	0.2			870.0
A.M.DP		4700.0				600.0	–	7.7×10^{-4}		
A.M.D			4300.0				250	–	126.0	
A.M.E				73,000				16.0	–	8935.6
A.M.T*					73,000	1.1			9243.8	–

The conditions are [ATP] = 1 mM, [ADP] = 10 μM, [Pi] = 1 mM, and [actin] = 1 mM.

where τ_1 is the torque experience by the trailing head and $\Delta\theta_p$ is the strain in the *binding pocket*. τ_1 can be computed from $\tau_1 = -\partial E_l/\partial\theta_1$, although $\Delta\theta_p$ is usually an unknown parameter.

With the addition of E_l and E_z to the total energy, the detailed balance condition must satisfy

$$\frac{k_{s_i\to s_i'}}{k_{s_i'\to s_i}} = \exp[\beta(E(\theta_1, \theta_2, s_1, s_2) - E(\theta_1, \theta_2, s_1', s_2))], \quad (17)$$

where E is the total energy of the system. However, since E_l is independent of s_i and E_z is only present when both heads are bound to actin, most of the rate expressions are largely unmodified. The crucial change occurs for binding and unbinding to actin. In the M.DP-state, in the absence of any stored elastic energy, the measured free energy change for binding to actin is 6 k_BT. With elastic coupling between the heads, the free energy change must be modified to include the elastic energy of the myosin complex before and after binding. The elastic energy before binding is given by

$$\Delta E_s(\theta_1, \theta_2, s_1, s_2) = E_0(\theta_1, s_1) + E_0(\theta_2, s_2) + E_l'(\theta_1, F), \quad (18)$$

where E_l' is the elastic energy of a single light-chain. After binding to actin, the elastic energy becomes

$$\Delta E_b(\theta_1, \theta_2, s_1, s_2) = E_0(\theta_1, s_1) + E_0(\theta_2, s_2) + E_z(z) + E_l(\theta_1, \theta_2, F, z). \quad (19)$$

$\Delta E_b - \Delta E_s$ is the additional free energy changes before and after binding. (See Fig. 4.) With these changes, we expect the transition state energy for binding to actin to change as well. A simple interpolation formula yields

$$E^\dagger = \lambda(\Delta E_b - \Delta E_s) - \Delta E_s, \quad (20)$$

where λ is somewhere between 0 and 1. We have taken $\lambda = 0.6$. The transition state energy as a function of the binding location, z, is shown in Fig. 5 *A*. We see that the preferred binding site is always $z = 36$ nm regardless of the external force. However, the energy difference between forward and backward binding becomes smaller with increasing load force.

The new reaction rate for binding to actin is therefore

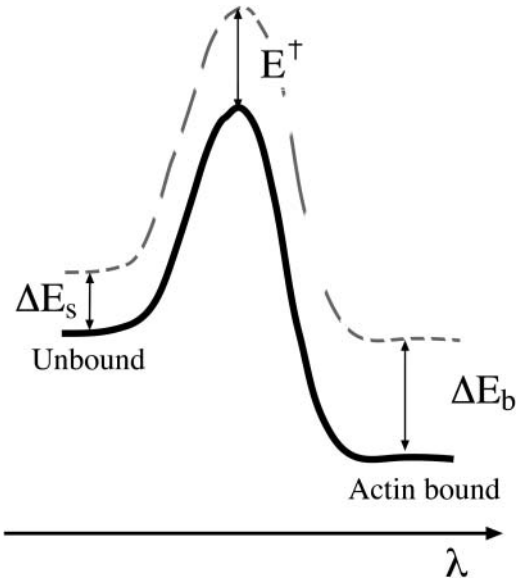

FIGURE 4 The transition state energy for binding to actin, $E^\dagger$, is determined by the elastic energy of the complex before (ΔE_s) and after (ΔE_b) binding.

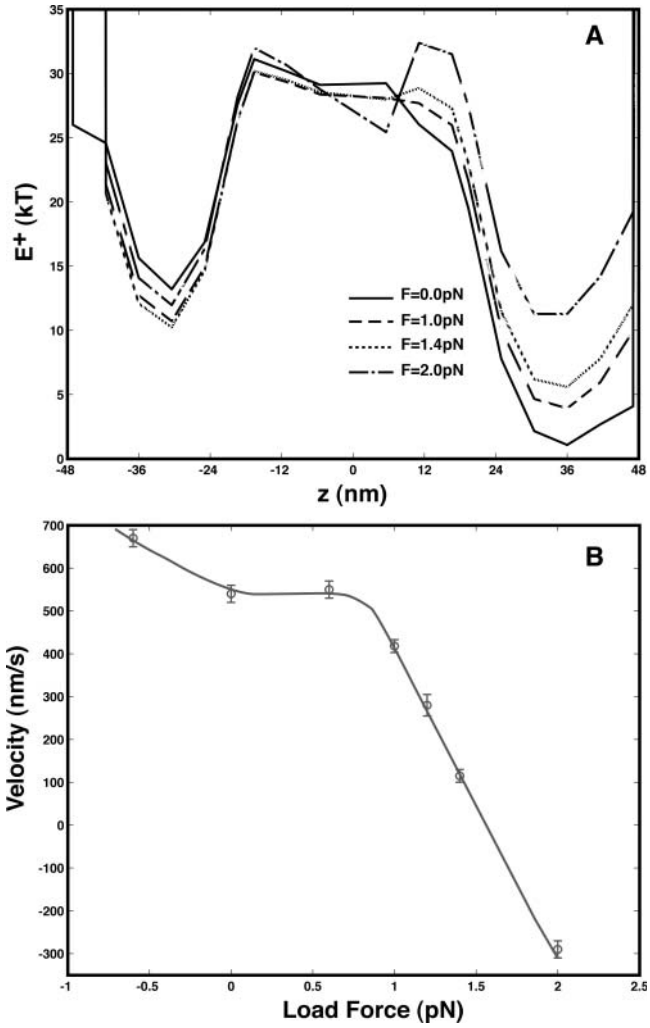

FIGURE 5 (*A*) The change in the transition state energy, $E^\dagger(z)$, for the leading head binding to actin. The value $E^\dagger$ is a function of z and (θ_1, θ_2). For this plot, (θ_1, θ_2) are chosen to be at the equilibrium position just before both heads are bound. The preferred binding location is always at 36 nm. The relative probability of binding to a different site is $e^{-\beta(E^\dagger(z')-E^\dagger(z))}$. (*B*) Force versus velocity curve for myosin-V. The symbols are from our Monte Carlo simulations. The line through the symbol is simply a guide for the eye. The predicted stall force is ~1.7 pN.

$$k_{\mathrm{M.}*\rightarrow\mathrm{A.M.}*} = k^0_{\mathrm{M.}*\rightarrow\mathrm{A.M.}*}\exp[-\beta(E^{\dagger}(\theta_1, \theta_2, z) - \Delta E_{\mathrm{s}})], \quad (21)$$

and it is a function of z. The unbinding rate from actin is also accordingly modified as

$$k_{\mathrm{A.M.}*\rightarrow\mathrm{M.}*} = k^0_{\mathrm{A.M.}*\rightarrow\mathrm{M.}*}\exp[-\beta(E^{\dagger}(\theta_1, \theta_2, z) - \Delta E_{\mathrm{b}})]. \quad (22)$$

As $E^{\dagger}$ increases, binding to actin also slows down. In the actual simulation, all possible binding sites are included. Due to fluctuations, it is possible to bind to an unfavorable binding site.

MODEL RESULTS

Having specified the elastic energy of the myosin-V complex and the chemical reaction rates, we convert Eq. 1 to an equivalent set of Fokker-Planck equations. We solve the dynamics by discretizing (θ_1, θ_2) and allow the system to stochastically progress through a four-dimensional-state space: (θ_1, θ_2, s_1, s_2). At any given moment, the system can change θ_{i} or s_{i}. We denote the position of the myosin heads as z_1 and z_2. The position of point C is Z. For any given state of myosin-V, we can obtain the geometrical shapes of the connecting light-chains. When both heads are bound to actin, Z is given by the equilibrium configuration of $E_{\mathrm{l}}(\theta_1, \theta_2, z, F)$. For a singly bound myosin with θ_1, Z is given by the equilibrium configuration of $E'_{\mathrm{l}}(\theta_1, F)$, whereas θ_2 simply fluctuates independently of θ_1.

The Monte Carlo procedure for computing myosin-V dynamics is explained in detail in the Appendix. Fig. 6 *A* shows a typical trajectory of Z versus time. The trajectory is for the wild-type myosin-V. Fig. 6 *B* shows the probability distribution of the step-size. Closer examination reveals that a single 36-nm step is sometimes separated into two substeps of 25 nm and 11 nm. The 11-nm substep is due to relaxation of the light-chains immediately after actin binding. The 25-nm substep is due to the powerstroke in the leading head after the trailing head releases from actin. The 36-nm step is the sum of the two substeps when binding occurs very rapidly.

The most favorable kinetic pathway for myosin-V is shown as the red path in Fig. 2. This result is the natural outcome of our model given the measured rate constants. Other kinetic pathways are also possible, particularly the pathway where M.ADP.Pi binds to actin. These pathways are in agreement with recent experimental findings (Baker et al., 2004).

Fig. 5 *B* shows the computed force versus velocity curve for myosin-V. The predicted stall force is 1.7 pN. Stall occurs when the actin binding rate to the $z = -36$-nm position becomes comparable to that of $z = 36$ nm. At forces <1 pN, the myosin-V velocity is not affected by the load force. This is because ADP release is the rate-limiting step in the trailing leg. However, for forces >1 pN, binding to actin becomes rate-limiting. The preferred binding site is relatively independent of the applied force, as evident in the transition state energy as a function of the binding site in Fig. 5 *A*. As the load force increases, the relative energy of binding to $z = 36$ nm becomes closer to that of $z = -36$ nm. The height of the curves also increases, indicating progressively slower actin binding rates.

Due to fluctuations in the angular positions and the elastic energy in the light-chains, the walking steps of myosin-V are not uniform. It is possible to observe an occasional backward step. Backward steps often occur when a slightly unfavorable configuration is reached before binding. The actin binding rate as a function of the binding site in Fig. 5 *A* shows the relative probabilities to bind to unfavorable sites. Substeps are also evident from the step-size distributions. The peaks in the step-size distributions are also relatively independent of the load force. However, as the force increases, the probability of seeing a backward step becomes more significant. At stall, there are just as many forward steps as backward steps. At stall, the motor is also not tightly coupled: ATP hydrolysis occurs without net forward motion.

The predicted stall force in our model is below the quoted value of 3 pN (Mehta et al., 1999). If the average step size remains 36 nm at 3 pN, then the thermodynamic efficiency of the motor approaches 100%. The kinetic measurements suggests that this cannot be the case. For instance, the transition from ATP to ADP.Pi lowers the free energy by 8 $k_{\mathrm{B}}T$. This step cannot perform any work in the direction of forward motion. Therefore, the free energy drop is lost, suggesting the efficiency is $\ll$100%. In our model, the powerstroke occurs after Pi release with a free energy drop of 12 $k_{\mathrm{B}}T$. The thermodynamics efficiency is 50%, completely consistent with the obtained stall force. In the measurement, the stall force is estimated from the dwell times preceding the *forward* steps. In our model calculations, we see that near stall, there is equal probability of stepping in both directions. Thus, the stall force for myosin-V requires further careful measurement.

CONCLUSIONS

The model presented here shows that a mechanical picture of myosin-V can capture most of the observed experimental data; however, the mechanical properties of the motor subunits had to be estimated. The stiffness of the light-chains, for example, is a crucial parameter in the model. We note that independent experimental estimates indicate $l_{\mathrm{p}} =$ 100 nm (Howard and Spudich, 1996). Thus, our parameter choice is in good agreement with experiment. The mechanical strain energy, E_{z}, due to binding away from 36 nm is important as well. Measurements of these properties are needed. The current model also neglects the dynamics of actin completely. It is conceivable that ATP hydrolysis in actin also plays a role, although we have shown that all of the experimental data can be explained without invoking actin ATP hydrolysis.

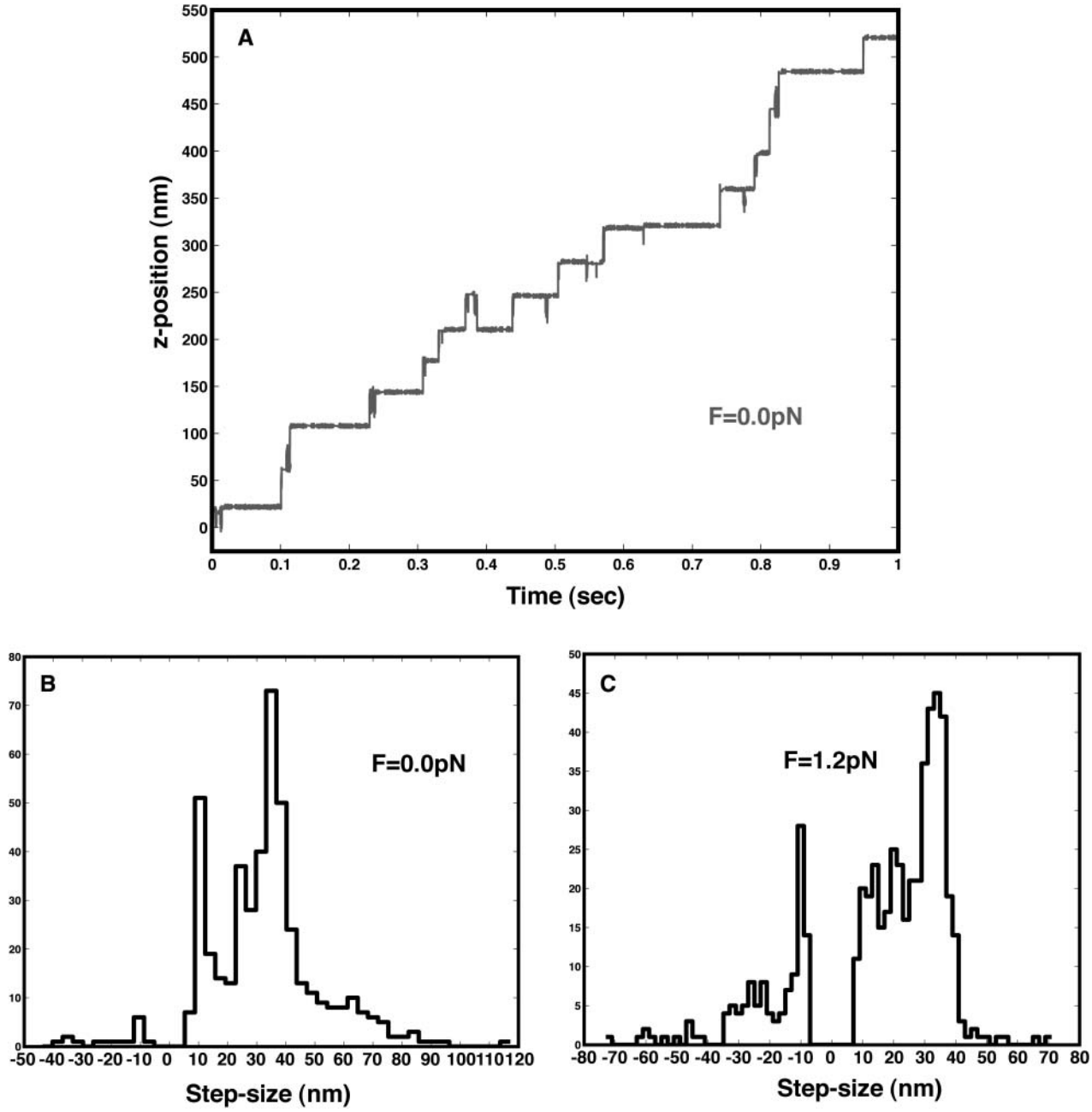

FIGURE 6 (*A*) A trajectory of myosin-V, showing the position of joint *C* along the *z* axis. The load force is absent for this case. (*B* and *C*) The step-size distributions of myosin-V for $F = 0.0$ pN and $F = 1.2$ pN. To simulate experimental conditions, the computed trajectories are windowed with a time-resolution of 1 ms. The step-size distributions have distinct peaks, indicative of substeps. The substeps, which can be seen from the trajectories, are 11 nm, 25 nm, and 36 nm. The step-size distribution changes as load force is increased. For example, there are more frequent backward steps. However, the 11-nm, 25-nm, and 36-nm substeps remain the same.

Our model makes several predictions that awaits experimental confirmation. For instance, we predict that at stall, the motor is not tightly coupled. The stall force is also quite low, $\approx$1.7 pN. At stall, forward and backward binding probabilities become comparable. We also made postulates regarding the shape of $E_0(\theta_i, s)$. By gathering statistics from the fluctuations in the myosin-V conformation, these quantities can perhaps be measured. Finally, we postulate that ADP release is a sharp function of the conformation. External forces on the lever-arm (or light-chains) can change the ADP release rates dramatically. We also have shown that the unidirectional stepping motion of myosin-V is due to the conformation-dependent ADP release. Experimental evidence indeed supports this hypothesis (Veigel et al., 2001),

although more quantitative measurements will further test the validity of the proposed model.

APPENDIX 1: COMPUTER SIMULATION PROCEDURE

Simulations of myosin-V dynamics can be carried out using Eq. 1 of the main text. Alternatively, a Fokker-Planck equation can be defined for the probability density $\rho(\theta_1, \theta_2, s_1, s_2)$. Assuming that the diffusion matrix is diagonal, the following equation describes the time evolution of the probability density

$$\frac{\partial \rho}{\partial t} = \sum_{i=1}^{2} \frac{1}{\zeta_i} \frac{\partial}{\partial \theta_i} \left[\frac{\partial E}{\partial \theta_i} \rho(\theta_1, \theta_2, s_1, s_2) + D_i \frac{\partial \rho}{\partial \theta_i} \right] + \sum_{s_1', s_2'=1}^{N} N k_{s_1, s_2 \leftarrow s_1', s_2'}(\theta_1, \theta_2) \rho(\theta_1, \theta_2, s_1', s_2'), \quad \text{(A1)}$$

where E is the total free energy of the myosin-V complex and $k_{s_1,s_2 \leftarrow s_1',s_2'}$ is the same rate matrix appearing in Eq. 1 of the main text. The diffusion constants $D_{1,2}$ describe the rotational diffusion of the light-chains. They are related to the friction coefficients via the Stokes-Einstein relation $D_i = k_B T/\zeta_i$. Strictly speaking, the diffusions of the light-chain filaments are not independent. We have ignored any hydrodynamic coupling between the filaments. An estimate of the diffusion constant is

$$D_i = k_B T \left(\frac{3\log(L/2r_0) - 0.447}{4\pi\eta L^3} \right), \quad \text{(A2)}$$

where L and r_0 are the length and radius of the light-chains respectively and η is the viscosity of water. (The numerical values of these parameters are given in Table 2.) A quick estimate gives $D_i \approx 5.5 \times 10^4 \text{rad}^2/\text{s}$. It is evident that the diffusion process is very much faster than the rate of kinetic transitions. Our results do not depend sensitively on the value of the diffusion constant.

Instead of solving the multidimensional Fokker-Planck equation, we compute a stochastic trajectory of myosin-V by discretizing the θ_1 and θ_2 spaces. The diffusion process in the angular space is modeled as Markov transitions between discrete angular states. This simulation procedure has been described before (Sun et al., 2004). In the discretized form, the Fokker-Planck equation becomes

$$\frac{\partial \tilde{\rho}_\alpha}{\partial t} = \sum_\beta \tilde{K}_{\alpha\beta} \rho_\beta, \quad \text{(A3)}$$

where the Greek indices α and β label states of the myosin-V system specified by $(\theta_{1,n}, \theta_{2,m}, s_1, s_2)$ where $\theta_{1,n}$ is the n^{th} discrete state of θ_1. Transitions can only occur by changing one of the four possible variables. The transition rate for $\alpha = (\theta_{1,n}, \theta_{2,m}, s_1, s_2)$ to $\beta = (\theta_{1,n+1}, \theta_{2,m}, s_1, s_2)$ is given by

$$\tilde{K}_{\alpha,\beta} = \frac{D_1}{\Delta\theta_1^2} \frac{E(\theta_{1,n+1}, \theta_2) - E(\theta_{1,n}, \theta_2)}{\exp[(E(\theta_{1,n+1}, \theta_2) - E(\theta_{1,n}, \theta_2))/k_B T] - 1}. \quad \text{(A4)}$$

The transition rate from β to α is given by

$$\tilde{K}_{\beta,\alpha} = -\frac{D_1}{\Delta\theta_1^2} \frac{E(\theta_{1,n+1}, \theta_2) - E(\theta_{1,n}, \theta_2)}{\exp[-(E(\theta_{1,n+1}, \theta_2) - E(\theta_{1,n}, \theta_2))/k_B T] - 1}. \quad \text{(A5)}$$

These transition rates ensure

$$\frac{\tilde{K}_{\alpha,\beta}}{\tilde{K}_{\beta,\alpha}} = \exp\left[\frac{E(\theta_{1,n}, \theta_2) - E(\theta_{1,n+1}, \theta_2)}{k_B T} \right]. \quad \text{(A6)}$$

We now give an example sequence of events. Let us start with one actin-bound myosin head with ADP in the catalytic site, where the other myosin head is free and has ATP in the catalytic site. In this situation, there are 23 accessible states. Four states represent $\pm\Delta\theta$ changes in θ_1 and θ_2. The bound head can also proceed to three other chemical states: (M.D, A.M.DP, and A.M.E). The free myosin head has 16 accessible states. Two of the 16 are changes in the catalytic site: (M.T* and M.DP). The other 14 are the possible actin binding sites. The rate constants for all the possible change are computed. The sum of the 23 rate constants is $\kappa = \sum_{\alpha=1}^{23} \tilde{K}_\alpha$. A random number, Δt, is chosen from the exponential distribution,

$$P(\Delta t) = e^{-\kappa t}. \quad \text{(A7)}$$

This gives the time when a state change occurs. To determine the destination state, another random number is chosen from the interval 0–1 and compared with the ratio $\tilde{K}_\alpha/\kappa$. The simulation procedure is similar to the Gillespie algorithm (Gillespie, 1977), although this method was first suggested by Bortz et al. (1975).

When only one myosin head is bound to actin, the other light-chain is free to diffuse rapidly. In our model, we do not explicitly simulate this diffusion process. Since the diffusion is rapid, the rate is not limited by the mean-passage time to reach a particular binding site. Rather, the rate is determined by the overall elastic energy of the motor. We treat the binding of the leading head as a rate process with rate constants determined by $E^\dagger(z, \theta_1, \theta_2)$.

APPENDIX 2: ADDITIONAL RESULTS

We have made animations of myosin-V movement based on our theoretical model. The animated movies are available for download at http://pegasus.me.jhu.edu/~seansun/MyosinV.htm. The movies are for 0.0-pN and 1.0-pN load conditions. The movies show the myosin-V configuration in the ABC plane at 10-ms intervals.

Since we do not simulate the free myosin head explicitly, in the movie it is shown as a stationary vertical post. In reality, the free myosin head is rapidly diffusing through medium. The binding rate to actin is not limited by the mean-passage time to the binding sites.

The authors thank James Sellers, Claudia Veigel, and Peter Knight for helpful discussions.

This work was supported by the Johns Hopkins Whiting School of Engineering and the Whitaker Foundation Biomedical Engineering Leadership Award.

REFERENCES

Baker, J., E. Krementsova, G. Kennedy, A. Armstrong, K. Trybus, and D. Warshaw. 2004. Myosin-V processivity: multiple kinetic pathways for head-to-head coordination. *Proc. Natl. Acad. Sci. USA*. 101:5542–5546.

Bortz, A., M. Kalos, and J. Lebowitz. 1975. A new algorithm for Monte Carlo simulation of Ising spin systems. *J. Comp. Phys*. 17:10–18.

Burgess, S., M. Walker, F. Wang, J. Sellers, H. White, P. Knight, and J. Trinick. 2002. The prepower stroke conformation of myosin-V. *J. Cell. Biol*. 159:983–991.

Bustamante, C., D. Keller, and G. Oster. 2001. The physics of molecular motors. *Acc. Chem. Res*. 34:412–420.

de la Cruz, E., A. Wells, S. Rosenfeld, M. Ostap, and H. Sweeney. 1999. The kinetic mechanism of myosin-V. *Proc. Natl. Acad. Sci. USA*. 96: 13726–13731.

Doi, M., and S. F. Edwards. 1986. The theory of polymer dynamics. *In* International Series of Monographs on Physics. Oxford University Press, New York.

Gillespie, D. 1977. Exact stochastic simulation of coupled chemical reactions. *J. Phys. Chem*. 81:2340–2361.

Howard, J. 2001. Mechanics of Motor Proteins and the Cytoskeleton. Sinauer Associates, Sunderland, MA.

Howard, J., and J. A. Spudich. 1996. Is the lever arm of myosin a molecular elastic element? *Proc. Natl. Acad. Sci. USA*. 93:4462–4464.

Houdusse, A., A. Szent-Gyorgyi, and C. Cohen. 2000. Three conformational states of scallop S1. *Proc. Natl. Acad. Sci. USA*. 97:11238–11243.

Ishii, Y., and T. Yanagida. 2002. A new view concerning an actomyosin motor. *Cell. Mol. Life Sci.* 59:1767–1770.

Kolomeisky, A., and M. E. Fisher. 2003. A simple kinetic model describes the processivity of myosin-V. *Biophys. J.* 84:1642–1650.

Langford, G. 2002. Myosin-V, a versatile motor for short-range vesicle transport. *Traffic*. 3:859–865.

Mehta, A., R. Rock, M. Rief, J. Spudich, M. Mooseker, and R. Cheney. 1999. Myosin-V is a processive actin-based motor. *Nature*. 400:590–593.

Mogilner, A., H. Wang, T. Elston, and G. Oster. 2002. Molecular motors: theory and experiment. *In* Computational Cell Biology. C. Fall, E. Marland, J. Wagner, and J. Tyson, editors. Springer-Verlag, New York.

Purcell, T., C. Morris, J. Spudich, and H. Sweeney. 2002. Role of the lever arm in the processive stepping of myosin-V. *Proc. Natl. Acad. Sci USA*. 99:14159–14164.

Raymond, I., H. Holden, M. Whittaker, C. Yohn, M. Lorenz, K. Holmes, and R. Milligan. 1993. Structure of the actin-myosin complex and its implications for muscle contraction. *Science*. 261:58–65.

Rief, M., R. Rock, A. Mehta, M. Mooseker, R. Cheney, and J. Spudich. 2000. Myosin-V stepping kinetics: a molecular model for processivity. *Proc. Natl. Acad. Sci. USA*. 97:9482–9486.

Risken, H. 1989. The Fokker-Planck Equation, Springer-Verlag, Berlin and Heidelberg.

Sun, S. X., H. Wang, and G. Oster. 2004. Asymmetry in the F_1-ATPase and its implications for the rotational cycle. *Biophys. J.* 83:1373–1384.

Tanaka, H., K. Homma, A. Iwane, E. Katayma, R. Ikebe, J. Saito, T. Yanagida, and M. Ikebe. 2002. The motor domain determines the large step of myosin-V. *Nature*. 415:192–195.

Veigel, C., F. Wang, M. Bartoo, J. Sellers, and J. Molloy. 2001. The gated gait of the processive molecular motor, myosin-V. *Nat. Cell Biol*. 4:59–65.

Walker, M., S. Burgess, J. Sellers, F. Wang, J. Hammer, J. Trinick, and P. Knight. 2000. Two-headed binding of a processive myosin to F-actin. *Nature*. 405:804–807.

Wang, H., and G. Oster. 1998. Energy transduction in the F_1-motor of ATP synthase. *Nature*. 396:279–282.

Yildiz, A., J. Forkey, S. McKinney, T. Ha, Y. Goldman, and P. Selvin. 2003. Myosin-V walks hand-over-hand: single fluorophore imagining with 1.5-nm localization. *Science*. 300:2061–2065.